Separation of grain boundary effects and intrinsic properties in perovskite-like Gd0.6Y0.4BaCo2O5.5 using high-frequency dielectric spectroscopy

Vid Bobnar, Peter Lunkenheimer, Michail Paraskevopoulos, Alois Loidl

Separation of grain boundary effects and intrinsic properties in perovskite-like $Gd_{0.6}Y_{0.4}BaCo_2O_{5.5}$ using high-frequency dielectric spectroscopy

V. Bobnar,* P. Lunkenheimer, M. Paraskevopoulos, and A. Loidl

Experimentalphysik V, Elektronische Korrelationen und Magnetismus, Institut für Physik, Universität Augsburg,
D-86135 Augsburg, Germany

The dielectric response of $Gd_{0.6}Y_{0.4}BaCo_2O_{5.5}$, which undergoes a sequence of magnetic and electronic phase transitions, has been investigated in the radio-frequency range from 1 MHz to 1.8 GHz in order to separate the intrinsic properties from grain boundary and sample-electrode interface effects. Analysis of the measured response, showing the characteristics of a damped resonator, reveals the intrinsic dc resistivity, which cannot be detected using the standard four-point measurement method. From the skin-effect-governed dielectric response the temperature dependence of the magnetic permeability was determined.

I. INTRODUCTION

The discovery of colossal magnetoresistance (MR) in perovskite-like manganese oxides[1] renewed interest in the properties of transition-metal oxides. Exciting ground states in these materials result from the competition of spin, charge, and orbital and structural degrees of freedom. Of special interest are the perovskite-type cobalt oxides, which reveal, depending on the relative strengths of crystal-field effects and Hund's rule coupling, different spin states and, in some cases, even temperature-dependent high-spin to low-spin transitions.[2–4] Recently, special attention was paid to the oxygen-deficient layered family of $RBaCo_2O_{6-x}$, where R is a rare-earth ion.[4–9] The structure of these compounds is derived from the perovskite structure via ordering of R and Ba cations into layers along the c axis and removing oxygen exclusively from the R layer. Hence the stacking sequence along the c axis can be described as —[BaO]—[CoO$_2$] —[RO$_{1-x}$]−[CoO$_2$]—. In addition to large MR effects, for $x \approx 0.5$, using four-point dc resistivity measurements, also a metal-insulator (MI) transition was detected at temperatures 310–360 K.[4–9]

When compared to the manganites, significant differences show up in the phenomenology of the sequence of phase transitions. While the temperature dependence of the magnetization looks very similar to that of the half-doped manganites,[10] the nature of phase transitions must be completely different. In cobaltites, the MI transition, yielding a step-like increase of the resistance by one order of magnitude, is connected with a structural phase transition indicative of orbital order and probably connected with a spin-state transition.[9] The latter shows up as a change of slope in the paramagnetic susceptibility only. The two succeeding magnetic transitions can hardly be detected in the resistance. In manganites the MI transition is driven by double exchange (DE) and is directly coupled with a paramagnetic (PM) to ferromagnetic (FM) transition, while charge order drives the antiferromagnetic (AFM) transition. It has been proposed that DE is also the driving force for the PM to FM transition in cobaltites, but due to the charge carrier localization, DE is overwhelmed by superexchange (SE) interactions, yielding an AFM ground state.[9] However, it remains unclear why no anomalies can be detected in the resistance at the PM to FM phase transition.

To shed some light on the nature of these phase transitions we performed detailed dielectric measurements on this class of compounds, focusing on a new member of this family, namely $Gd_{0.6}Y_{0.4}BaCo_2O_{5.5}$. The synthesis, structural details, and the magnetic properties are described in a separate publication: Magnetization and four-point dc measurements revealed that $Gd_{0.6}Y_{0.4}BaCo_2O_{5.5}$ undergoes a sequence of MI, FM, and AFM phase transitions at temperatures of $T_{MI} \approx 340$ K, $T_c \approx 290$ K, and $T_N \approx 270$ K, respectively.[11]

Dielectric measurements are an important tool to characterize MI transition, where a diverging dielectric constant is expected.[12] Numerous reports of extremely high dielectric constants in transition-metal oxides point in this direction; however, in ceramic samples a careful analysis is needed to separate intrinsic electronic properties from grain boundary effects. Indeed, in the manganites it is well known that the electrical transport is highly influenced by grain boundary resistance and that band bending and space charge effects are important for their physics.[13] By performing high-frequency impedance measurements, contributions from contacts, bulk, and grain boundaries can be separated. Thus, the main emphasis of this work is to characterize the electronic bulk properties using dielectric spectroscopy and to check for a diverging dielectric constant at the MI transition. In addition, we want to examine the occurrence of hopping conduction of localized charge carriers, which leads to characteristic contributions to the ac conductivity.

II. EXPERIMENTAL PROCEDURES

The polycrystalline $Gd_{0.6}Y_{0.4}BaCo_2O_{5.5}$ samples were prepared using conventional mixed oxide synthesis.[11] Ultrapure oxide powders were dried, mixed in the appropriate amounts, and carefully ball milled to ensure homogeneous samples. Pressed pallets were sintered at 1200 °C for 5 h and then slowly cooled down to room temperature. The oxygen
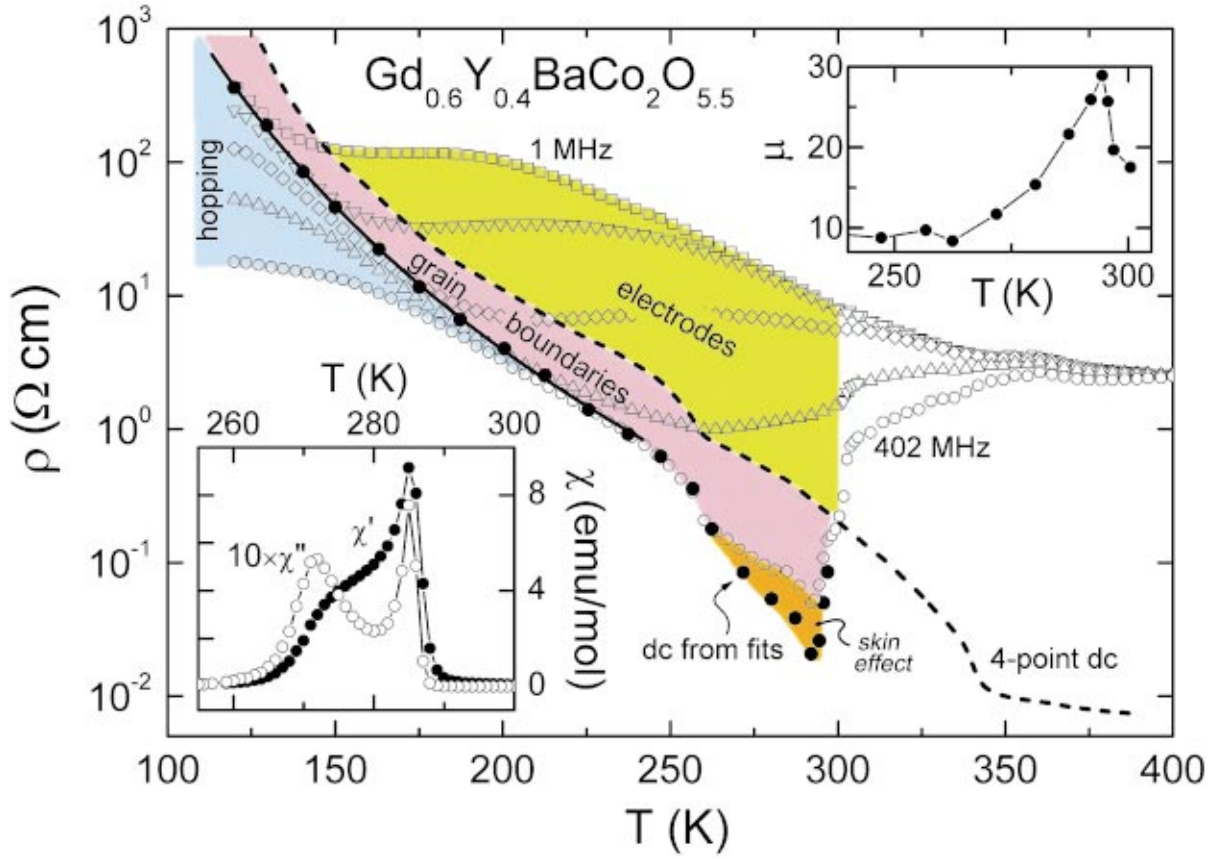
FIG. 1. (Color) Temperature dependence of the resistivity of $Gd_{0.6}Y_{0.4}BaCo_2O_{5.5}$. Open symbols: ac resistivity ρ' for different frequencies: 1 MHz ($\square$), 3.85 MHz (∇), 17.3 MHz ($\diamond$), 77.3 MHz ($\triangle$), and 402 MHz ($\bigcirc$). Dashed line: four-point dc resistivity. Solid circles: intrinsic dc resistivity as deduced from the equivalent-circuit analysis of the frequency-dependent data (Figs. 2 and 3). Solid line: fit of the intrinsic dc conductivity to the variable-range hopping model. The colored regions indicate the different contributions to the overall response, as explained in the text (for $T>300$ K no clear identification is possible). The lower inset shows a representative result of an ac magnetic susceptibility measurement for the determination of the magnetic phase transition temperatures. The upper inset shows the temperature dependence of the magnetic permeability μ, determined from the intrinsic dc resistivity and skin-effect-induced frequency dependence of the resistance.

content of the samples was determined thermogravimetrically with an accuracy of approx 0.4%. The magnetic susceptibility and magnetization were measured using a superconducting quantum interference device (SQUID) magnetometer (0–50 kOe, 1.5 K$<T<$400 K). In the lower inset to Fig. 1 we show a representative result of an ac susceptibility measurement. Two peaks in the imaginary part χ'' and a peak and shoulder in the real part χ' of the susceptibility characterize the transitions from the PM to the FM state ($T_c \approx 290$ K) and from the FM to the AFM phase ($T_N \approx 270$ K).

Dielectric measurements were performed employing a reflectometric technique, as described in Ref. 14. Since this technique requires a two-point contact configuration, electrodes contribute to the measured overall response.

III. RESULTS AND ANALYSIS

Figure 1 shows the temperature dependence of the dc resistivity ρ_{dc}^{4p} (dashed line), measured in a standard four-point configuration, compared to the resistivity ρ', measured at

various frequencies between 1 MHz and 402 MHz (open symbols). ρ_{dc}^{4p} shows a significant increase at $T_{MI} \approx 340$ K; however, only a small anomaly is observed at T_N, and no anomaly at all is detected at T_c. The ac measurements lead to a drastically different temperature dependence of ρ'. While no transitions are detected at 1 MHz, at the highest frequencies significant anomalies, both at T_N and at T_c, can be observed. Especially, on approaching T_c the impedance at microwave frequencies is strongly reduced, a behavior that to our knowledge has never been observed so far. While this behavior involves contributions from bulk and grain boundaries, it is clear that the intrinsic electronic properties have to change considerably at T_c. In order to explain this phenomenon we performed a detailed analysis of the high-frequency dielectric response in $Gd_{0.6}Y_{0.4}BaCo_2O_{5.5}$.

Figure 2 shows the frequency dependence of the dielectric constant ε' and conductivity σ', measured at several temperatures. At lower temperatures the data reveal the characteristics of an overdamped resonator. ε' spectra at these temperatures are shown in the inset, since they differ significantly from those obtained in the temperature region
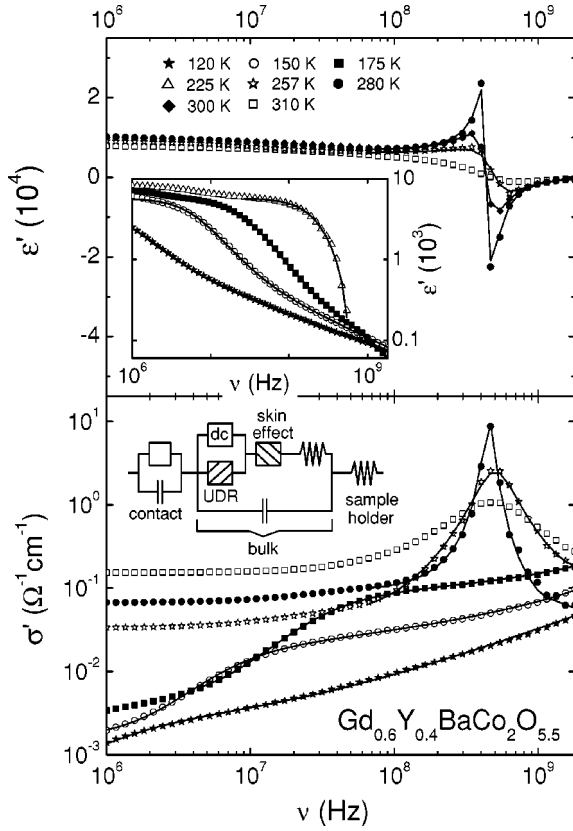
FIG. 2. Frequency dependence of the dielectric constant ε' and conductivity σ' measured at several temperatures in $Gd_{0.6}Y_{0.4}BaCo_2O_{5.5}$. The ε' data obtained at lower temperatures are shown in the inset. Solid lines through the experimental data are fits using the equivalent circuit, which is also indicated in the figure.

around the magnetic transitions, where the system behaves like an underdamped resonator.

At low temperatures, a distinctive downward step in ε' (inset to Fig. 2), which is accompanied by a step-like increase in σ', is observed. Since for low frequencies ε' approaches unreasonably high values and the corresponding peaks in $\varepsilon'' \sim \sigma'/\omega$ (not shown) follow a single-exponential Debye response, the origin of this behavior are contact contributions, rather than a dipolar relaxation process. Besides external contacts that, via the formation of Schottky diodes, lead to a thin depletion layer of low carrier concentration at the sample surface,[15] also internal contacts, i.e., grain boundaries, can drive such a behavior. Indeed, at $T > 150$ K two successive steps are observed (inset to Fig. 2), which we ascribe to the two types of contacts—external and internal. For high frequencies the capacitive contact barriers become successively shorted and the intrinsic response is detected. At temperatures below 200 K, following the contact steps, σ' approaches a plateau, which can be identified with the intrinsic "bulk" dc conductivity σ_{dc}. At higher frequencies σ' increases steeper again and concomitantly, following the contact step, ε' approaches a power-law decrease (see, e.g., the 120 K curve in the inset to Fig. 2). This intrinsic frequency dependence can be well described by the so-called universal dielectric response (UDR) with the addition of a dc conductivity[15]
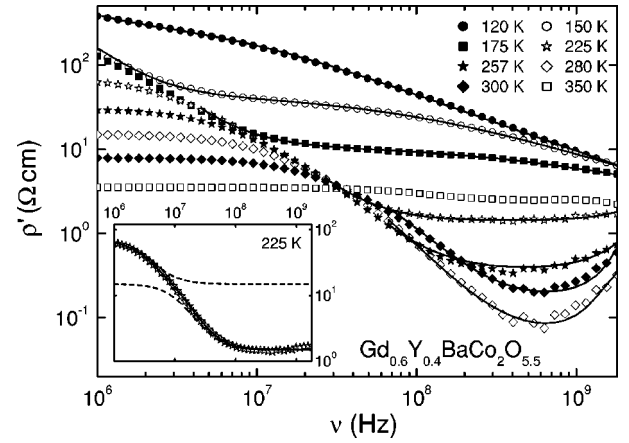

FIG. 3. Frequency dependence of the real part of the resistivity ρ'. Solid lines through the experimental data are fits using the equivalent circuit, presented in Fig. 2. The inset shows data at $T = 225$ K, fitted to an equivalent circuit consisting of two RC circuits in series to the intrinsic dc resistance. Dashed lines in the inset show the separate contributions from external and internal contacts.

$$\sigma' = \sigma_{dc} + \sigma_0 \omega^s, \quad \sigma'' = \omega \varepsilon_0 \varepsilon' = \tan(s\pi/2)\sigma_0 \omega^s, \quad (1)$$

with ε_0 being the permittivity of free space and $s < 1$. Several theoretical approaches deduce such a behavior from microscopic hopping transport properties, including thermal excitation over or tunneling through an energy barrier separating different sites of the localized charge carriers.[16]

With increasing temperatures, approaching the magnetic transitions, a peak in $\sigma'(\omega)$ develops and at the highest frequencies ε' becomes negative. This behavior of an underdamped resonator with a resonance frequency of several hundred MHz can be ascribed to the inductance L of the system in conjunction with high values of σ_{dc}.

In addition to the above-mentioned contributions, also the skin effect may play a role at high frequencies. The skin depth δ depends on the resistivity and magnetic permeability μ of the material as

$$\delta = [2\rho/\mu\mu_0\omega]^{1/2}, \quad (2)$$

where μ_0 is the permeability of free space. If δ reaches the order of the sample thickness, the reduction of the current-carrying cross section leads to an increase of the measured resistance.[17]

Figure 3 shows the frequency dependence of the real part of the resistivity ρ', which can be calculated from σ' and ε'. As the impedance of the inductance, $i\omega L$, contributes to the imaginary part only, the resonance dominating the high-temperature curves of $\sigma'(\omega)$ and $\varepsilon'(\omega)$ (cf. Fig. 2) plays no role in $\rho'(\omega)$. Instead, for $T \geq 225$ K a skin-effect-related increase of $\rho'(\omega)$ shows up at the highest frequencies, which can be ascribed to the elevated μ close to the magnetic transitions in conjunction with the relatively low resistivity.

In order to analyze the experimental data quantitatively, we have used the equivalent circuit, presented in Fig. 2. Internal contact contributions are modeled by a parallel RC circuit.[15,17,18] The intrinsic response of the sample is described by its dc conductance, the UDR, skin effect, and its

inductance and capacitance, the latter taking into account the high-frequency dielectric constant due to ionic and electronic polarization. Finally, the inductance of the sample holder is connected in series. It may be remarked that, depending on the temperature range, only part of different elements are in fact necessary for a description of the sample; e.g., at low temperatures the contact RC circuit can be omitted as the contact step has shifted out of the frequency window (cf. Figs. 2 and 3). The lines in Figs. 2 and 3 are fits using this equivalent circuit, performed simultaneously for ε' and σ'. At low temperatures the equivalent circuit leads to an excellent description of the complete spectra. However, with increasing temperature deviations appear at low frequencies. Here the contact steps, successively shifting into the frequency window, turn out to be too broad to be fitted satisfactorily by one contact step only and contributions both from external and internal contacts have to be considered. As an example, in the inset of Fig. 3 the $\rho'(\omega)$ curve at $T = 225$ K is fitted by an equivalent circuit consisting of two RC circuits connected in series to each other and to the bulk sample, which for simplicity is represented by a resistor only. The broad contact step can well be taken into account in this way (solid line). The dashed lines demonstrate the separate contributions from the external and internal contacts.

The most significant result of the equivalent-circuit analysis is the intrinsic dc resistivity ρ_{dc}^i. Its temperature dependence for $T < 300$ K is shown in Fig. 1 (solid circles). It exhibits values up to one decade lower than ρ_{dc}^{4p}. This can be ascribed to the grain boundaries that contribute to ρ_{dc}^{4p} as indicated by the purple region in Fig. 1. Only by high-frequency measurements can the intrinsic resistivity of these ceramic samples be detected. The 1 MHz curve for $T > 220$ K reflects the sum of external and internal contact resistances, the external contribution being indicated by the green region. For decreasing temperatures, ρ_{dc}^i is successively approached as the characteristic time constant of the circuit comes into the region of the inverse measurement frequency. For the higher frequencies, this happens for successively higher temperatures, and for the 402 MHz curve in the region 125 K $< T <$ 300 K, the contact capacitances are shorted and the intrinsic response is detected. This is also reflected by the coincidence of ρ_{dc}^i and ρ' (402 MHz) in the region 190 K $< T <$ 270 K. The deviations of the high-frequency curves from ρ_{dc}^i showing up at $T < 190$ K (blue region) are due to the UDR and indicate the importance of hopping of localized charge carriers in this region. This is corroborated by the temperature dependence of ρ_{dc}^i, which for $T < 230$ K can be described using the prediction of the variable-range hopping model, $\rho_{dc} \sim \exp(-T_0/T)^{1/4}$.[19] The deviation of ρ' (402 MHz) and ρ_{dc}^i showing up around the magnetic transitions can be ascribed to the skin effect, as indicated by the orange region. For this region, from the fits, via Eq. (2) the magnetic permeability can be determined (upper inset of Fig. 1),[17] exhibiting a pronounced peak at T_c and even a small anomaly at T_N.

At $T \gtrsim T_c$, the interpretation of the results is hampered by the fact that at high frequencies a mixture of intrinsic, contact-related, and skin effect contributions is actually measured, and the transition at T_c seems to affect all these contributions. Namely, the grain boundary contribution seems to diminish and the internal contact step moves to much higher frequencies. Nevertheless, from the equivalent-circuit analysis, significant information on $\rho_{dc}^i(T)$ can be obtained up to 300 K and at the PM to FM transition ρ_{dc}^i seems to reduce by at least a factor of 5. This fact implies that DE interactions in fact are responsible for the occurrence of FM in these compounds, as suggested by Moritomo *et al.*[9] The finding that for $T < T_c$, after the initial drop, ρ_{dc}^i increases again on decreasing temperature seems to support the view that DE interactions are suppressed due to carrier localization that sets in at T_{MI}.[9] In fact the hopping conduction of localized charge carriers is explicitly detected below 200 K and may play a role also at higher temperatures. Finally, at T_N SE interactions dominate, yielding the AFM ground state. However, it remains a puzzle why T_c cannot be detected at all in dc experiments. At T_c, grain boundary effects contribute ≈ 0.3 Ω cm to the total dc resistance, while ρ_{dc}^i just below T_c reaches value of some 10 mΩ only (cf. Fig. 1). Nevertheless, when ρ_{dc}^i is reduced at T_c, one expects to observe a kink in ρ_{dc}^{4p}. Its absence can only be explained by the fact that at T_c, at the same time while the intrinsic resistance decreases, the intergrain resistance increases, smearing out any clear anomaly. And indeed the onset of significant intergrain resistivity is well documented in a number of MR manganites.[13]

IV. CONCLUSIONS

In conclusion, by performing dielectric spectroscopy in the high-frequency range from 1 MHz to 1.8 GHz, the intrinsic properties were separated from the contributions of grain boundaries and sample-electrode interface in the layered perovskite $Gd_{0.6}Y_{0.4}BaCo_2O_{5.5}$. The intrinsic dc resistivity is significantly smaller than the resistivity determined by standard four-point measurements, for which grain boundary contributions dominate. In contrast to the four-point dc results, the ferromagnetic transition shows up as a pronounced anomaly in the resistivity measured in the 100 MHz range. From the analysis a decrease of the intrinsic dc resistivity at T_c, indicating the importance of DE interactions, can be suspected. At temperatures below 200 K, the hopping of localized charge carriers is detected, becoming the dominant charge transport process at low temperatures.

*On leave from Jožef Stefan Institute, Ljubljana, Slovenia.

[1] R. von Helmholt, J. Wecker, B. Holzapfel, L. Schultz, and K. Samwer, Phys. Rev. Lett. **71**, 2331 (1993); S. Jin, T. H. Tiefel, M. McCormack, R. A. Fastnacht, R. Ramesh, and L. H. Chen, Science **264**, 413 (1994).

[2] I. O. Troyanchuk, N. V. Kasper, D. D. Khalyavin, H. Szymczak, R. Szymczak, and M. Baran, Phys. Rev. Lett. **80**, 3380 (1998).

[3] Y. Moritomo, M. Takeo, X. J. Liu, T. Akimoto, and A. Nakamura, Phys. Rev. B **58**, R13 334 (1998).

[4] I. O. Troyanchuk, N. V. Kasper, D. D. Khalyavin, H. Szymczak, R. Szymczak, and M. Baran, Phys. Rev. B **58**, 2418 (1998).

[5] A. Maignan, C. Martin, D. Pelloquin, N. Nguyen, and B. Raveau, J. Solid State Chem. **142**, 247 (1999).

[6] T. Vogt, P. M. Woodward, P. Karen, B. A. Hunter, P. Henning, and A. R. Moodenbaugh, Phys. Rev. Lett. **84**, 2969 (2000).

[7] T. Saito, T. Arima, Y. Okimoto, and Y. Tokura, J. Phys. Soc. Jpn. **69**, 3525 (2000).

[8] W. S. Kim, E. O. Chi, H. S. Choi, N. H. Hur, S.-J. Oh, and H.-C. Ri, Solid State Commun. **116**, 609 (2000).

[9] Y. Moritomo, T. Akimoto, M. Takeo, A. Machida, E. Nishibori, M. Takata, M. Sakata, K. Ohoyama, and A. Nakamura, Phys. Rev. B **61**, R13 325 (2000).

[10] H. Kuwahara, Y. Tomioka, A. Asamitsu, Y. Moritomo, and Y. Tokura, Science **270**, 961 (1995).

[11] M. Paraskevopoulos *et al.* (unpublished).

[12] T. G. Castner, Philos. Mag. B **42**, 873 (1980); H. F. Hess, K. DeConde, T. F. Rosenbaum, and G. A. Thomas, Phys. Rev. B **25**, 5578 (1982).

[13] J. Klein, C. Höfener, S. Uhlenbruck, L. Alff, B. Büchner, and R. Gross, Europhys. Lett. **47**, 371 (1999); S. Lee, H. Y. Hwang, B. I. Shraiman, W. D. Ratcliff II, and S-W. Cheong, Phys. Rev. Lett. **82**, 4508 (1999).

[14] R. Böhmer, M. Maglione, P. Lunkenheimer, and A. Loidl, J. Appl. Phys. **65**, 901 (1989).

[15] A. K. Jonscher, *Dielectric Relaxations in Solids* (Chelsea Dielectrics Press, London, 1983).

[16] S. R. Elliott, Adv. Phys. **36**, 135 (1987).

[17] A. Seeger, P. Lunkenheimer, J. Hemberger, A. A. Mukhin, V. Yu. Ivanov, A. M. Balbashov, and A. Loidl, J. Phys.: Condens. Matter **11**, 3273 (1999).

[18] P. Lunkenheimer, M. Resch, A. Loidl, and Y. Hidaka, Phys. Rev. Lett. **69**, 498 (1992).

[19] N. F. Mott and E. A. Davis, *Electronic Processes in Non-Crystalline Materials* (Clarendon Press, Oxford, 1979).